THE PUBLISHING HOUSE
OF THE ROMANIAN ACADEMY

PROCEEDINGS OF THE ROMANIAN ACADEMY, Series A,
Volume 15, Number 3/2014, pp. 300–309

APPLICATION OF A GTN DAMAGE MODEL TO PREDICT THE FRACTURE OF METALLIC SHEETS SUBJECTED TO DEEP-DRAWING

Abdolvahed KAMI [1], Bijan MOLLAEI DARIANI [1], Ali SADOUGH VANINI [1], Dan-Sorin COMSA [2], Dorel BANABIC [2]

[1] Amirkabir University of Technology, Department of Mechanical Engineering, Tehran, Iran
[2] Technical University of Cluj-Napoca, CERTETA Research Centre, Cluj-Napoca, Romania
E-mail: dariani@aut.ac.ir

In this paper, an anisotropic formulation of the Gurson-Tvergaard-Needleman (GTN) damage model is used for simulating the deep-drawing of a rectangular box made from an AA6016-T4 metallic sheet. The model is implemented as a VUMAT routine in the ABAQUS/Explicit finite-element code. The material parameters involved in the constitutive relationships are determined by means of an identification procedure that combines the response surface methodology (RSM) and the simulation of a uniaxial tensile test. In order to assess the predictive performances of the GTN model, different levels of the blank-holding force are assumed in the finite-element analysis of the deep-drawing process. The comparison between the numerical results and experimental data shows not only a good accuracy of the fracture predictions, but also the capability of the GTN model to provide a realistic description of the material response during the whole forming process.

Key words: deep-drawing, fracture, GTN Damage model, anisotropy.

1. INTRODUCTION

Aluminium alloys have become attractive for the automotive industry mainly because of their light weight. In the form of cold rolled thin sheets, such materials are used to produce car body panels by deep-drawing operations. Because of their special anisotropy characteristics, sheets made from aluminium alloys are prone to fracture when large strains are induced during the forming process. In practical applications, it is very important to predict such undesirable phenomena. One of the theoretical models developed with this aim in view is due to Gurson [1]. According to Gurson's approach, the degradation of the load carrying capacity and finally the fracture of ductile metals are caused by the evolution of voids. In its original formulation, the model takes into account only the growth of pre-existing voids, without assuming any generative mechanisms. In order to overcome this limitation, Tvergaard and Needleman [2–4] proposed mathematical descriptions of the void nucleation and coalescence. This modified model is known as Gurson-Tvergaard-Needleman (GTN) damage model.

Both models (Gurson and GTN) assume that the metal matrix is isotropic and obeys the von Mises yield function. In fact, because of the cold rolling production procedure, sheet metals usually exhibit a non-negligible anisotropic behaviour. Many attempts have been made to include the anisotropy of the matrix material in the GTN model. Liao et al. [5] derived an approximate potential closed to the original Gurson formulation, in which the Hill's quadratic [6] and non-quadratic [7] anisotropic expressions of the equivalent stress are used to describe the anisotropy. They used anisotropy parameters defined as the ratio of the transverse plastic strain rate to the through-thickness plastic strain rate under in-plane uniaxial loading along different directions. Wang et al. [8] proposed to use the average anisotropy parameter instead of the directional parameters in the model proposed by Liao et al. [5]. Chen and Dong [9] extended the GTN model to characterize the matrix material through Hill quadratic [6] and Barlat-Lian 3-component [10] expressions of the equivalent stress. Chen and Dong [11] proposed extensions of the GTN potential based on Hill's quadratic anisotropic expression of the equivalent stress [6].

Various anisotropic GTN models have been successfully used for predicting the fracture occurrence in sheet metal forming processes [11–13]. In this paper, a GTN model based on Hill's quadratic expression of the equivalent stress is used for simulating the deep-drawing of a rectangular box made from an AA6016-T4 metallic sheet. The model is implemented as a VUMAT routine in the ABAQUS/Explicit finite-element code [14]. The material parameters involved in the constitutive relationships are determined by means of an identification procedure that combines the response surface methodology (RSM) and the simulation of a uniaxial tensile test.

2. GTN DAMAGE MODEL

2.1. GTN model based on HILL'48 expression of the equivqlent stress

As previously mentioned, both the original Gurson model [1] and the GTN version developed by Tvergaard and Needleman [2–4] assume the plastic isotropy of the matrix material. However, the experimental data obtained from mechanical tests show that cold rolled sheet metals are anisotropic bodies. In recent years, many attempts have been made to develop anisotropic formulations of the GTN model [5,8, 9, 11]. The expression of the equivalent stress proposed by Hill in 1948 [6] is able to give a sufficiently good description of the plastic anisotropy exhibited by the sheet metals used in industrial applications. This fact, as well as the computational efficiency ensured by its quadratic form, determined the authors to include Hill'48 equivalent stress in the ABAQUS/Explicit implementation of the GTN model.

Hill'48 equivalent stress is expressible as follows [6]:

$$\bar{\sigma} = \left[F(\sigma_{22} - \sigma_{33})^2 + G(\sigma_{33} - \sigma_{11})^2 + H(\sigma_{11} - \sigma_{22})^2 + 2L\sigma_{23}^2 + 2M\sigma_{31}^2 + 2N\sigma_{12}^2 \right]^{1/2}. \tag{1}$$

The quantities denoted as σ_{ij} (i, j = 1, 2, 3) in Eq. (1) are Cartesian components of a corotational Cauchy stress tensor expressed in a frame that follows the local rotation of the anisotropy axes, while F, G, H, L, M, and N are material constants. The parameters F, G, H, L, M, and N can be evaluated using different types of experimental data. In the case of metallic sheets, the standard identification procedure relies on the Lankford coefficients r_0, r_{45} and r_{90} obtained from uniaxial tensile tests performed on specimens cut at 0°, 45° and 90° with respect to the rolling directions. The following relationships can be used to evaluate the parameters F, G, H, L, M, and N when these coefficients are available:

$$\begin{aligned} &F = \frac{H}{r_{90}}, \quad G = \frac{H}{r_0}, \quad H = \frac{r_0}{r_0 + 1}, \\ &L = M = \frac{3}{2}, \quad N = \frac{(r_0 + r_{90})(2r_{45} + 1)}{2r_{90}(r_0 + 1)}. \end{aligned} \tag{2}$$

The general form of the GTN damage potential is:

$$\Phi = \left(\frac{\bar{\sigma}}{Y} \right)^2 + q_1 f^* \left[2\cosh\left(-q_2 \frac{3p}{2Y} \right) - \frac{q_3}{q_1} f^* \right] - 1, \tag{3}$$

where $\bar{\sigma}$ is the equivalent stress defined by Eq. (1),

$$p = -(\sigma_{11} + \sigma_{22} + \sigma_{33})/3 \tag{4}$$

is the hydrostatic pressure, Y is the yield stress of the matrix material defined as a function of the equivalent plastic strain $\bar{\varepsilon}^p$ by means of Swift's hardening law

$$Y(\bar{\varepsilon}^p) = K(\varepsilon_0 + \bar{\varepsilon}^p)^n, \tag{5}$$

and

$$f^* = \begin{cases} f, & \text{if} \quad f \le f_c, \\ f_c + \dfrac{f_f^* - f_c}{f_f - f_c}(f - f_c), & \text{if} \quad f_c < f < f_f, \\ f_f^*, & \text{if} \quad f \ge f_f \end{cases} \tag{6}$$

is a porosity parameter depending on the current void volume fraction f. The quantity f^* has been introduced by Tvergaard and Needleman [0] to describe the accelerated loss of load carrying capacity due to the coalescence of voids. All the other symbols occurring in Eqs (3), (5) and (6) are material constants.

The inequality $\Phi \le 0$ defines all the admissible stress states of the sheet metal. More precisely,

$$\begin{cases} \Phi < 0, & \text{in elastic states,} \\ \Phi = 0, & \text{in elastoplastic states.} \end{cases} \tag{7}$$

With this observation, the flow rule associated to the GTN potential can be expressed in the form

$$\dot{\boldsymbol{\varepsilon}}^{(p)} = \dot{\lambda}\frac{\partial \Phi}{\partial \boldsymbol{\sigma}}, \qquad \text{where} \begin{cases} \dot{\lambda} = 0, & \text{if } \Phi < 0, \\ \dot{\lambda} \ge 0, & \text{if } \Phi = 0. \end{cases} \tag{8}$$

In the above relationship, $\dot{\boldsymbol{\varepsilon}}^{(p)}$ is the plastic part of the strain rate tensor.

The change of the void volume fraction f is caused by the growth of the initial void volume fraction f_0 and the nucleation of new voids at the limits of the second phase particles and inclusions:

$$\dot{f} = \dot{f}_{growth} + \dot{f}_{nucleation} \tag{9}$$

where

$$\dot{f}_{growth} = (1-f)\left[\dot{\varepsilon}_{11}^{(p)} + \dot{\varepsilon}_{22}^{(p)} + \dot{\varepsilon}_{33}^{(p)}\right] \tag{10}$$

and

$$\dot{f}_{nucleation} = \frac{f_N}{S_N\sqrt{2\pi}} \exp\left[-\frac{1}{2}\left(\frac{\bar{\varepsilon}^{(p)} - \bar{\varepsilon}_N}{S_N}\right)^2\right]. \tag{11}$$

The quantities denoted as S_N, $\bar{\varepsilon}_N$ and f_N in Eq. (11) are also material constants that must be determined by identification.

2.2. Identification procedure

Among the material constants included in the constitutive relationships presented above, $q_1, q_2, q_3, f_0, f_c, f_f, f_N, S_N,$ and $\bar{\varepsilon}_N$ need a special attention, because the predictive performances of the GTN model are strongly dependent on their values. In general, an identification procedure that tries to determine all these parameters would be very inefficient because of the large amount of experimental data needed for calibration. On the other hand, the success of such an approach would be also improbable in many cases due to the non-uniqueness of the solution [15, 16]. Most of the researchers use the values proposed by Needleman and Tvergaard for q_1, q_2, q_3, S_N and $\bar{\varepsilon}_N$ parameters, namely, $q_1 = 1.5,\ q_2 = 1,$ $q_3 = q_1^2 = 2.25,\ S_N = 0.1,$ and $\bar{\varepsilon}_N = 0.3$ [0, 0]. In this paper, with the aim of simplifying the identification procedure, this approach will be adopted. As a consequence, only the remaining parameters $f_0, f_c, f_f,$ and f_N should be found. For their determination, the authors have developed an identification procedure based on the response surface methodology (RSM). A face centred central composite RSM design of experiments

has been implemented in the software package Design-Expert® (trial version 7.0.0). These experiments are uniaxial tensile tests as shown in Fig. 4. A total number of 27 experiments with different parameter (factor) combinations have been performed (see Table 1).

Table 1

Different values of the identification factors

Factor	Values		
f_0	0.0001	0.00055	0.001
f_N	0.001	0.0255	0.05
f_c	0.005	0.0275	0.05
f_f	0.06	0.13	0.2

The response of the experiments has been defined by means of Eq. (12), where $|\square|$ is the absolute value

$$\text{Response} = \sum_{i=1}^{n} \left| F_{exp} - F_{num} \right|_i . \tag{12}$$

The quantities denoted as F_{exp} and F_{num} in Eq. (12) are experimental and numerically predicted values of the tensile force acting on the specimen for different elongation stages individualized by the index *i*. The total elongation of the gauge (up to the fracture occurrence) was assumed to be 25 mm. One should mention that, in the experimental tensile tests, the fracture occurred at about 21.48 mm elongation for the specimens cut along the rolling direction. On the other hand, when using the RSM based identification procedure, different combinations of factors lead to different predictions for the fracture elongation (smaller than 21.48 mm or even larger than 30 mm). The authors noticed that the function expressed by Eq. (12) was able to provide quite reasonable values of the RSM design response when an "averaged" value of the fracture elongation of 25 mm was adopted. For all the experiments included in the RSM design, the values of the force were set to zero between the fracture point and the maximum elongation of 25 mm. The summation limit *n* in Eq. (12) was set to 1000. The results of the identification procedure for the case of an AA6016-T4 sheet metal (1 mm thickness) will be presented in §5.1.

3. EXPERIMENTS

3.1. Uniaxial tensile tests

The material adopted in the experimental research is an AA6016-T4 metallic sheet with the nominal thickness of 1 mm. AA6016-T4 is an Al-Mg-Si alloy currently used in the automotive industry for the production of deep-drawn outer panels. This material has a good formability in the T4 temper state, low springback, good weldability and high corrosion resistance. The uniaxial tensile tests have been performed on specimens cut at 0, 45 and 90° with respect to the rolling direction. In all cases, rectangular specimens with the dimensions $200\,\text{mm} \times 20\,\text{mm} \times 1\,\text{mm}$ have been used. Their elongation has been measured with an extensometer having the gauge length of 80 mm. The testing methodology is presented in [0]. Figure 1 shows some representative results of the uniaxial tensile tests. A summary of the material properties obtained from these experiments is given in Table 2: Lankford coefficients (r), conventional yield stress ($R_{p0.2}$) and ultimate tensile strength (R_m).

The material curves recorded by the tensile testing equipment in the case of the specimens cut along the rolling direction have been also used for the calibration of Swift's hardening law (see Eq. (5)). The authors have developed an identification procedure based on the least squares method. The following values of the coefficients K, ε_0 and n have been obtained in this way: $K = 525.77$ MPa, $\varepsilon_0 = 0.011252$ and $n = 0.2704$.

Finally, the uniaxial tensile tests have also provided the elastic properties of the material. The average values of Young's modulus (E) and Poison's ratio (ν) are 70 GPa and 0.33, respectively.

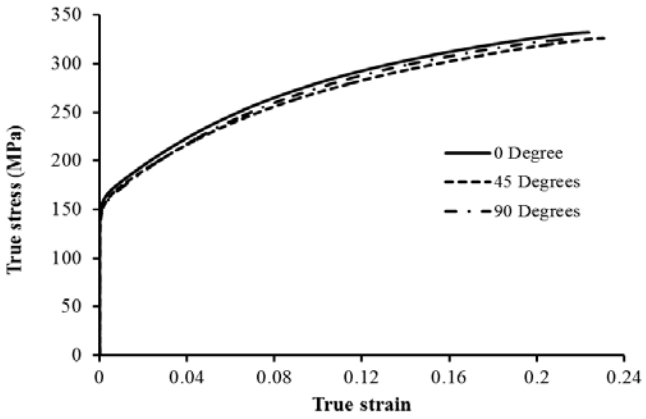

Fig. 1 – Material curves obtained by uniaxial tensile tests performed at 0°, 45° and 90° with respect to the rolling direction (AA6016-T4 sheet metal; 1 mm thickness).

Table 2

Mechanical properties of the AA6016-T4 sheet metal (1 mm thickness)

Orientation	r	$R_{p0.2}$ [MPa]	R_m [MPa]
0°	0.5529	158.07	264.89
45°	0.4091	152.25	259.84
90°	0.5497	154.75	263.32

3.2. Deep-drawing equipament

Fig. 2 shows the tooling setup used in the deep-drawing experiments [20]. The tests have been performed on circular blanks with 85 mm diameter lubricated on both faces with a mixture of oil and graphite. In all cases, the punch speed has been set to a constant value of 33 mm/min. Deep drawing tools have been installed on the Erichsen universal testing machine (Fig. 3) which ensures a hydraulic control of the blank holding force and punch displacement. Different values of the blank holding force have been adopted in the experiments. For values lower than 4 kN, the flange has been affected by wrinkling, while holding forces greater than 10 kN have caused the fracture of the deep-drawn parts. The experimental results obtained in the case of the maximum holding force (10 kN) will be used for comparison with the predictions of the GTN model.

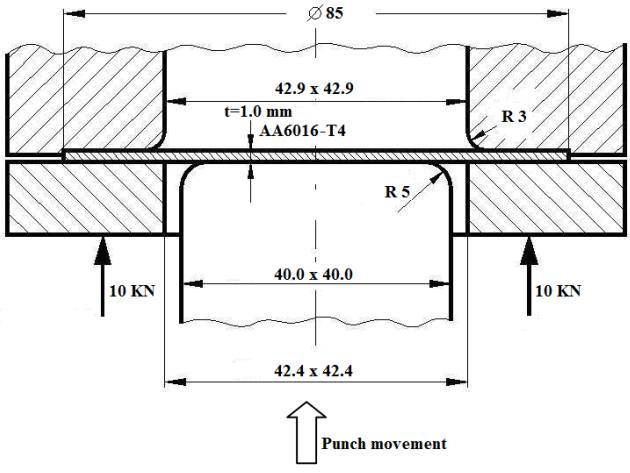

Fig. 2 – Tooling setup used in the deep-drawing experiments [20].

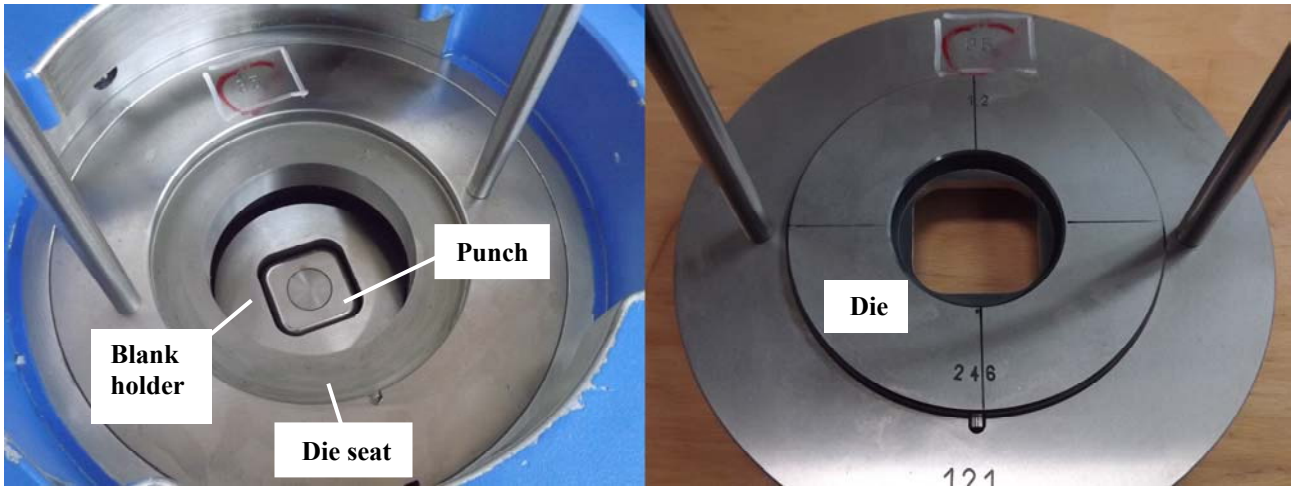

Fig. 3 – Deep-drawing tools installed on the Erichsen universal testing machine.

4. NUMERICAL ANALYSIS

The numerical analysis has been focused on the finite-element simulation of the uniaxial tensile tests and deep-drawing experiments. In all cases, the commercial code ABAQUS/Explicit has been used in combination with the anisotropic GTN damage model implemented as a VUMAT routine.

4.1. Simulation of the uniaxial tensile tests

As discussed in the previous sections, the RSM design of experiments has been used for the identification of the GTN model. The response values for this design have been calculated from force vs. displacement curves corresponding to uniaxial tensile loads. For this reason, uniaxial tensile tests have been numerically simulated. The finite element model used in the numerical analysis has been reduced to the gauge section of the rectangular specimens. The boundary conditions and dimensions of the analysis domain are shown in Fig. 4. A total displacement of 25 mm has been applied at the right end of the finite element mesh. Hexahedral elements with 8 nodes (C3D8R) and the edge size of 0.5 mm have been used for meshing the analysis domain.

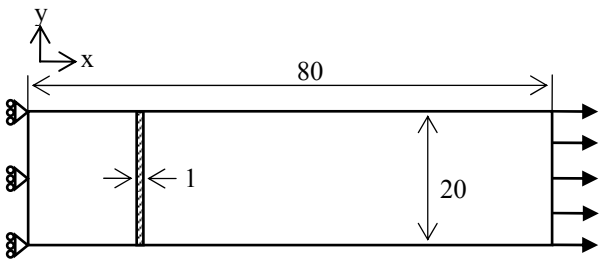

Fig. 4 – Geometry and boundary conditions of the AA6016-T4 specimen (simulation of a uniaxial tensile test).

4.2. Simulation of deep-drawing experiments

The essential surfaces of the tools (punch, die and blank holder) have been meshed using rigid shell elements (R3D4), while solid deformable elements (8-node hexahedra C3D8R with the average edge size of 0.5 mm) have been adopted for meshing the circular blank. Due to the geometric and mechanical symmetry of the deep-drawing process, only one quarter of the tool surfaces and blank volume have been included in the finite-element model. Three layers of solid elements have been generated in the thickness direction of the blank. A concentrated force of 2.5 kN has been applied to the reference point of the blank holder (one quarter

of actual blank holding force – 10 kN). The die has been kept fixed in its position, the punch and the blank holder being allowed to perform vertical translations. The frictional contact between blank and tools has been modelled using a penalty formulation. Taking into account the lubrication conditions of the laboratory experiments, the friction coefficient has been set to a value of 0.05 on all the contact surfaces. The numerical simulation of the deep-drawing process has been divided in two steps: in the first stage, the blank holding force is raised up to its maximum force (2.5 kN); in the next stage, the punch performs a vertical translation until the occurrence of the fracture in the blank.

5. RESULTS AND DISCUSSIONS

5.1. Parameter identification

As previously mentioned, the parameters f_0, f_c, f_f and f_N have been determined using an identification procedure based on the response surface methodology. The optimum values of the parameters provided by this procedure are the following ones: $f_0 = 0.000242$, $f_c = 0.047674$, $f_f = 0.2$ and $f_N = 0.041546$. Numerical simulations of uniaxial tensile tests have been performed using these material constants. Figure 5 shows a comparison between the force *vs*. elongation curve predicted by the GTN model and the experimental curve obtained by averaging the results of the uniaxial tensile tests performed along the rolling direction. One may easily notice that the numerical results are in very good agreement with the experimental data. This fact allows concluding that the values of the parameters f_0, f_c, f_f and f_N obtained by identification are representative for the AA6016-T4 sheet metal with the nominal thickness of 1 mm and can be used for the simulation of more complex forming processes.

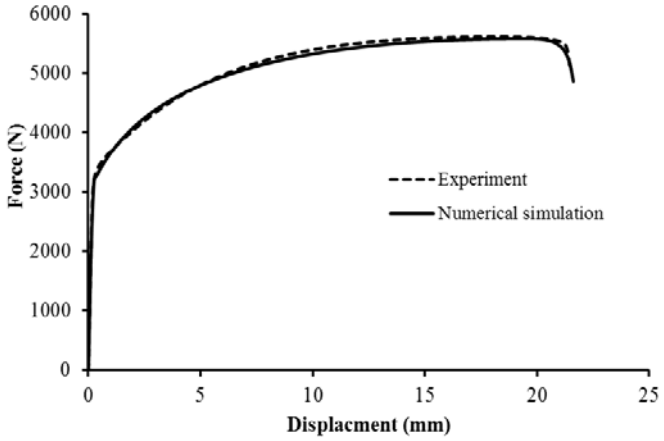

Fig. 5 – Force vs elongation curves corresponding to uniaxial tensile tests performed along the rolling direction (comparison between experimental results and numerical predictions).

Fig. 6 shows a comparison between the tensile specimens fractured during the experimental tests and the numerical simulations. The rectangle in Fig. 6a contains the gauge section which is used in the finite element analysis. After analysing this data, one may conclude that the numerical model with the identified values of the parameters is able to predict the fracture occurrence with an acceptable accuracy. The coloured map in Fig. 6b shows the distribution of the total void volume fraction (denoted as SDV2 in the legend).

Figure 7 presents several stages of a tensile test simulated with ABAQUS/Explicit: uniform distribution of the void volume fraction in a stage preceding the strain localization – Fig. 7a; different stages of the strain localization process characterized by an accelerated evolution of the void volume fraction that tends to accumulate in a narrow region as a consequence of the coalescence phenomenon – Fig. 7b, c, d.

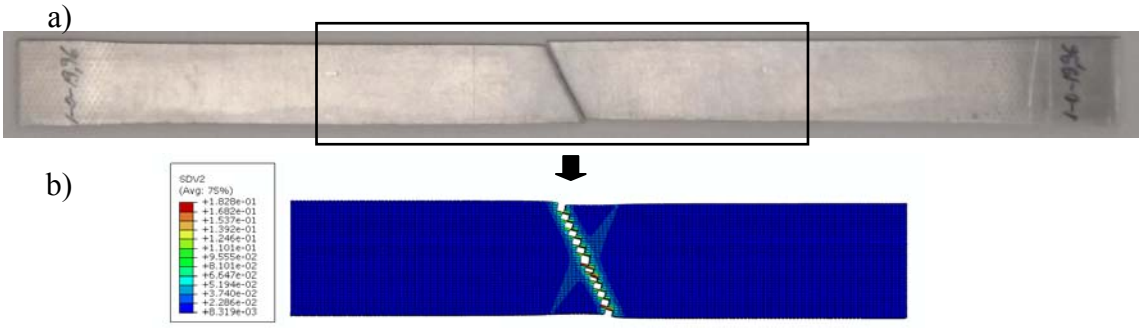

Fig. 6 – Tensile specimen after fracture a) experiment; b) numerical simulation.

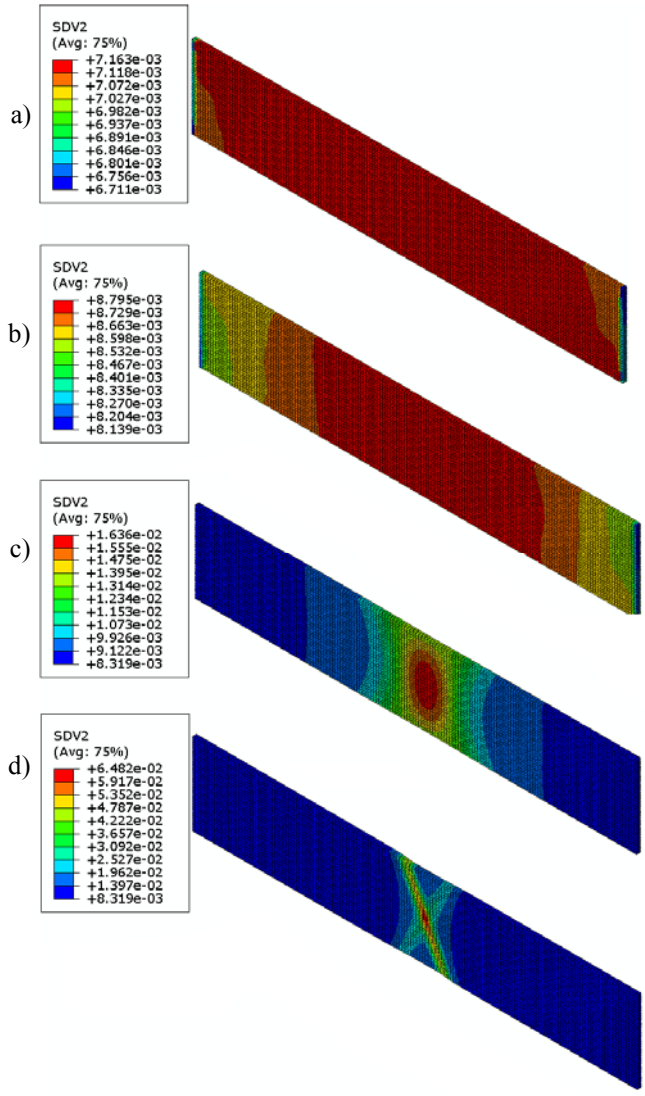

Fig. 7 – Evolution of the void volume fraction during the uniaxial tensile test:
a) 17.99 mm; b) 19.48 mm; c) 20.47 mm; d) 21.22 mm elongation.

5.2. Simulation of the deep-drawing process

Fig. 8 illustrates the fracture of the AA6016-T4 metallic sheet during the deep-drawing tests performed with a blank holding force set to 10 kN. This figure compares the predictions of the anisotropic GTN model with the experimental data. One may notice that fracture path has almost the same shape and position in both images.

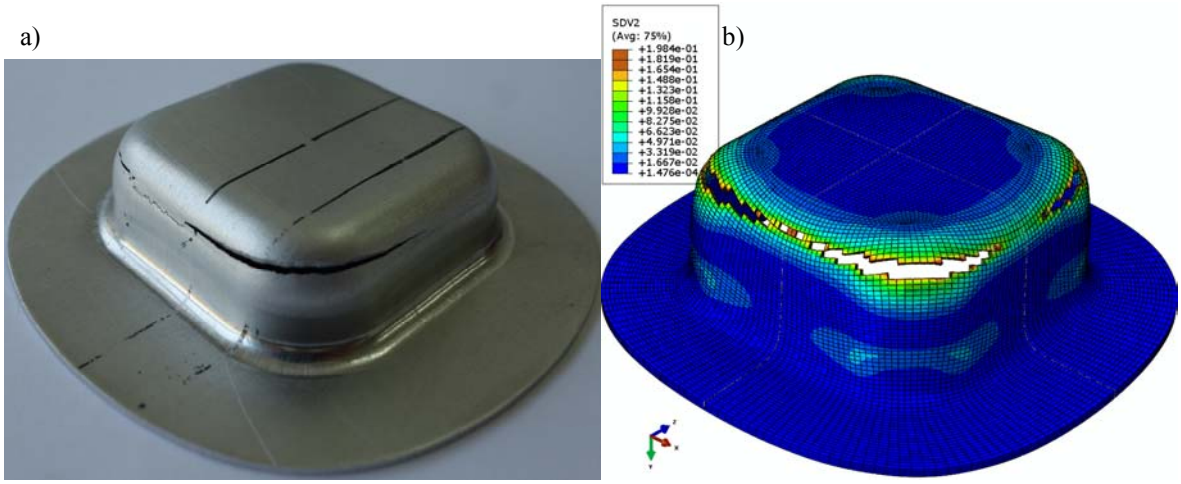

Fig. 8 – Fractured specimens: a) experiment; b) numerical simulation.

Fig. 9 shows the evolution of the punch force during the deep-drawing process. Experimental data and numerical predictions are superimposed on the same diagram. One may notice that the maximum level of the punch force predicted by ABAQUS/Explicit (32.27 kN) is almost equal to the experimentally determined value (34.24 kN). The diagram also allows the evaluation of the drawing depth at which the fracture occurs. This depth corresponds to the sudden drop of the punch force towards zero: 17.90 mm – predicted by ABAQUS/Explicit, in very good agreement with the depth of 18.70 mm measured on the experimental curve.

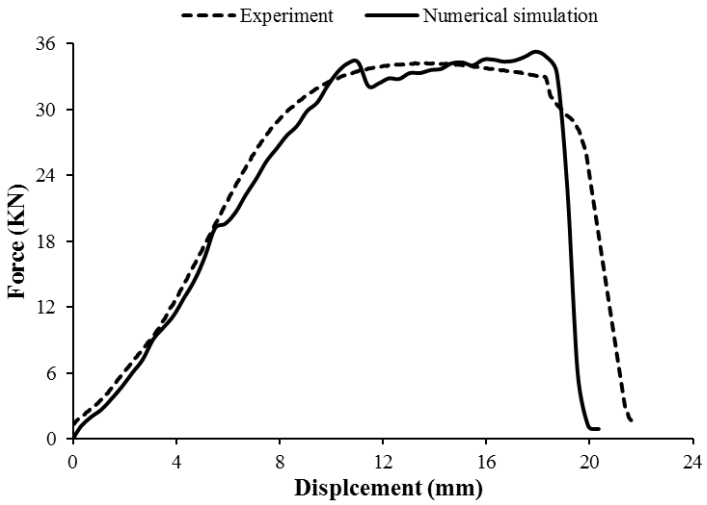

Fig. 9 – Comparison of forming forces for blank holder of 10 kN.

6. CONCLUSIONS

The GTN damage model combined with Hill'48 expression of the equivalent stress has been used to predict the fracture of metallic sheets subjected to deep-drawing. The material constants included in the formulation of the damage model have been calibrated using the response surface methodology. The identification procedure is quick and straightforward as the required material parameters are derived by conducting simple uniaxial tensile tests and their numerical simulation. The finite element simulation of a deep-drawing process has proved not only a good accuracy of the fracture predictions, but also the capability of the GTN model to provide a realistic description of the material response during the whole forming process (relative errors smaller than 5 % in the prediction of the maximum punch force and the drawing depth at which the fracture occurs).

REFERENCES

1. GURSON, A.L., *Continuum theory of ductile rupture by void nucleation and growth. Part I – Yield criteria and flow rules for porous ductile media*, J. Eng. Mater. Tech., **99**, *1*, pp. 2–15, 1977.
2. TVERGAARD, V., *Influence of voids on shear band instabilities under plane strain conditions*, Int. J. Fract., **17**, *4*, pp. 389–407, 1981.
3. TVERGAARD, V., *On localization in ductile materials containing spherical voids*, Int. J. Fract., **18**, *4*, pp. 237–252, 1982.
4. TVERGAARD, V., NEEDLEMAN, A., *Analysis of the cup-cone fracture in a round tensile bar*, Acta Metallurgica, **32**, *1*, pp. 157–169, 1984.
5. LIAO, K.C., PAN, J., TANG, S.C., *Approximate yield criteria for anisotropic porous ductile sheet metals*, Mech. Mater., **26**, *4*, pp. 213–226, 1997.
6. HILL, R., *A theory of the yielding and plastic flow of anisotropic metals*, Roy. Soc. London Proc. A, **193**, *1033*, pp. 281–297, 1948.
7. HILL, R., *Theoretical plasticity of textured aggregates*, Math. Proc. Camb. Phil., **85**, *1*, pp. 179–191, 1979.
8. WANG, D.A., PAN, J., LIU, S.D., *An Anisotropic Gurson Yield Criterion for Porous Ductile Sheet Metals with Planar Anisotropy*, Int. J. Damage Mech., **13**, *1*, pp. 7–33, 2004.
9. CHEN, Z., DONG, X., *Comparison of GTN damage models for sheet metal forming*, J. Shanghai Jiaotong Univ. (Science), **13**, *6*, pp. 739–743, 2008.
10. BARLAT, F., LIAN, K., *Plastic behavior and stretchability of sheet metals. Part I: A yield function for orthotropic sheets under plane stress conditions*, Int. J. Plasticity, **5**, *1*, pp. 51–66, 1989.
11. CHEN, Z., DONG, X., *The GTN damage model based on Hill'48 anisotropic yield criterion and its application in sheet metal forming*, Comput. Mater. Sci., **44**, *3*, pp. 1013–1021, 2009.
12. BRUNET, M., MORESTIN, F., MGUIL, S., *The Prediction of Necking and Failure in 3 D. Sheet Forming Analysis Using Damage Variable*, J. Phys. IV France, **06**, *C6*, pp. C6-473-C6-482,1996.
13. BRUNET, M., MGUIL, S., MORESTIN, F., *Analytical and experimental studies of necking in sheet metal forming processes*, J. Mater. Proc. Tech., **80-81**, pp. 40–46, 1998.
14. HIBBITT, K., SORENSEN, *ABAQUS/Standard user's manual*, Version 6.11, 2011.
15. LI, Z.H., BILBY, B.A., HOWARD, I.C., *A study of the internal parameters of ductile damage theory*, Fatigue Fract. Eng. M., **17**, *9*, pp. 1075–1087, 1994.
16. ZHANG, Z.L., *A sensitivity analysis of material parameters for the gurson constitutive model*, Fatigue Fract. Eng. M., **19**, *5*, pp. 561–570, 1996.
17. NEEDLEMAN, A., TVERGAARD, V., *An analysis of ductile rupture in notched bars*, J. Mech. Phys. Solids, **32**, *6*, pp. 461–490, 1984.
18. BENSEDDIQ, N., IMAD, A., *A ductile fracture analysis using a local damage model*, Int. J. Pres. Ves. Pip., **85**, *4*, pp. 219–227, 2008.
19. PĂRĂIANU, L., BANABIC, B., *Characterization of the plastic behaviour of AA6016-T4 aluminium alloy*, Adv. Eng. Forum, **8-9**, pp. 293–300, 2013.
20. NICODIM, I., CIOBANU, I., BANABIC, D., *Effect of the constitutive law on the prediction of the wall thickness distribution of square cup*, Proceedings of 11th International MeTM Conference, Cluj-Napoca, Romania, 17–19 October 2013, pp. 173–176.

Received April 3, 2014